Journal Pre-proof

Effect of sputter pressure on microstructure and properties of β -Ta thin films

Elizabeth A.I. Ellis, Markus Chmielus, Shangchen Han, Shefford P. Baker

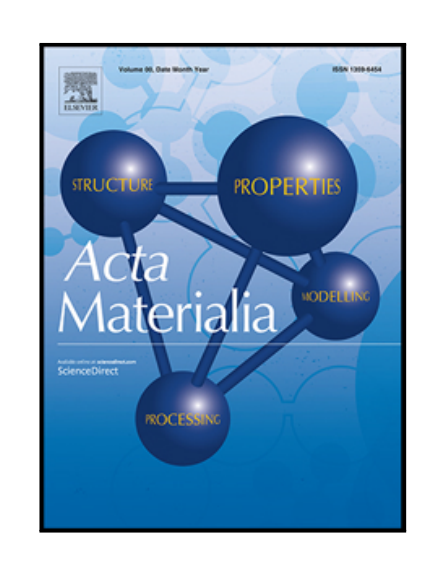
PII: \$1359-6454(19)30734-7

DOI: https://doi.org/10.1016/j.actamat.2019.10.056

Reference: AM 15632

To appear in: Acta Materialia

Received date: 27 July 2019
Revised date: 28 October 2019
Accepted date: 29 October 2019



Please cite this article as: Elizabeth A.I. Ellis, Markus Chmielus, Shangchen Han, Shefford P. Baker, Effect of sputter pressure on microstructure and properties of β -Ta thin films, *Acta Materialia* (2019), doi: https://doi.org/10.1016/j.actamat.2019.10.056

This is a PDF file of an article that has undergone enhancements after acceptance, such as the addition of a cover page and metadata, and formatting for readability, but it is not yet the definitive version of record. This version will undergo additional copyediting, typesetting and review before it is published in its final form, but we are providing this version to give early visibility of the article. Please note that, during the production process, errors may be discovered which could affect the content, and all legal disclaimers that apply to the journal pertain.

© 2019 Published by Elsevier Ltd on behalf of Acta Materialia Inc.

Journal Pre-proof

Effect of sputter pressure on microstructure and properties of β -Ta thin films

Elizabeth A. I. Ellis^{1,*}, Markus Chmielus^{2,3}, Shangchen Han² and Shefford P. Baker^{1,2}

- 1. Cornell University, Sibley School of Mechanical and Aerospace Engineering, Upson Hall, Ithaca, NY 14853 USA
- 2. Cornell University, Department of Materials Science and Engineering, Bard Hall, Ithaca, NY 14853 USA
- 3. University of Pittsburgh, Department of Mechanical Engineering & Materials Science, Benedum Hall, Pittsburgh, PA 15261 USA
- * Now at Oak Ridge National Laboratory, Oak Ridge, TN 37830

ABSTRACT

Tantalum thin films may be deposited in two phases. The stable bulk alpha phase is well known, but the metastable tetragonal beta phase is relatively poorly understood. We reported previously on a series of 100% β -Ta films deposited under varying sputter pressures in a low-oxygen environment, and discussed texture, stresses, and phase selection. Here, we discuss microstructure, morphology, and properties of these same β -Ta films. Grain size increases with sputter pressure, which can be explained by the energies of incident species at the growing film. Mechanical properties were measured by nanoindentation. Hardness decreases with grain size in accordance with the Hall-Petch relation while comparison of indentation modulus with biaxial modulus measurements indicates that the β phase is elastically anisotropic, and much stiffer in the [001] direction than in others. Finally, a canonical resistivity value for virtually oxygen-free, 100% β -Ta films of 169 ± 5 μ Ω cm is reported for the first time.

2

1. INTRODUCTION

Tantalum thin films are widely used in industry and therefore widely studied (e.g. [1–10]). Until recently, however, there has been greater interest in the stable BCC α phase of tantalum than in the metastable β phase that appears only in thin films. The two phases are quite different and are therefore suited to different applications. While α -Ta films are used in a variety of applications such as wear-resistant coatings and diffusion barriers for Cu-Si interconnects, β -Ta has generally been desired only for Ta thin film resistors. However, the recent discovery of a giant spin Hall effect in β -Ta may be important for the development of next-generation magnetoresistive memory technologies [11], and has renewed interest in this phase.

Because α -Ta has been preferred in many applications for many years, relatively little is known about the structure and properties of β -Ta films. It is well-known that β -Ta has a high electrical resistivity compared to the conductive α phase, but reported values vary widely, from 112 $\mu\Omega$ cm [9] to 1500 $\mu\Omega$ cm [8]. The origins of these variations are unknown, but they have been attributed to included α -Ta [10], grain size [8], and oxygen content [12] in the films. Similarly, hardness has been reported to vary from \sim 12 GPa [3] to \sim 20 GPa [6] with variations attributed to stresses [3], strain rate [4,6] and grain size [5]. While there are few reports of elastic properties, Young's modulus has been reported to be as high as 194 GPa [5] or to vary with grain size and texture over the range 166-183 GPa [4]. Of course, properties are expected to depend intimately on structure and composition, but because systematic studies of pure β -Ta films are rare, the literature on the properties of β -Ta remains fragmentary and the actual correlations between composition, structure, and properties are unknown. Some reasons for this include that Ta films have been produced on a variety of different substrates, using a wide range of deposition parameters, and including a number of different impurities.

To explore synthesis-structure-properties relationships more systematically, we prepared a set of β -Ta thin films by sputtering in an ultra-high-vacuum system with sputter gas pressure, p_{Ar} , ranging from 0.3 to 2.2 Pa while holding other deposition parameters constant and taking steps to minimize impurities. In a previous article [13], we reported that the stresses varied dramatically, from –1360 to + 1140 MPa over this pressure range and that the resulting x-ray diffraction (XRD) peak shifts allowed us to show that the films were virtually 100% β -Ta with a single (002) fiber texture component that broadens significantly with p_{Ar} . These results, combined with an analysis of the distributions of energy and incident angle of species arriving at the substrate, allowed us to propose a new model for phase selection in Ta films that explains virtually all findings to date.

In the present article, we report on the microstructure, morphology, and properties of these films. By carefully controlling the deposition environment to ensure that all films are pure β Ta, we are able to explain a growth phenomenon (increasing grain size with $p_{\rm Ar}$) that has been reported but not explained, provide an explanation for the reported variations in hardness of the β phase, provide an estimate for the indentation modulus, and to provide, for the first time, a canonical value of the resistivity of β -Ta films with neither α -Ta content nor oxygen contamination.

2. EXPERIMENTS AND RESULTS

A series of seven β -Ta films were deposited under a range of sputter pressures from 0.3 to 2.2 Pa. Microstructure was characterized using scanning electron microscopy (SEM), mechanical properties were measured using nanoindentation, and resistivity was measured using a four-point probe.

2.1. Film deposition, stresses, phase, and texture

Film deposition, phase, and texture are described in detail elsewhere [13]. Briefly, β -Ta thin films were produced by DC magnetron sputtering from a 99.95% pure Ta target in a custom ultra-high vacuum (UHV) deposition chamber [14] at each of 7 selected Ar sputter gas pressures, p_{Ar} = 0.3, 0.5, 1.1, 1.6, 1.9, 2.0, and 2.2 Pa (2, 4, 8, 12, 14, 15, and 16 mTorr). Substrates were (100) Si wafers with native oxide, 100 mm in diameter, and 525 μ m thick. Efforts were made to minimize the effects of impurities, particularly oxygen content. The base pressure was 2.7 × 10⁻⁶ Pa (2 × 10⁻⁸ Torr) or better. The working gas was ultra-high-purity (UHP–99.999%) Ar that was additionally filtered to reduce oxygen content to less than 1 ppb. Before deposition, substrates were plasma cleaned for 1 min using a 25 W RF bias in 1.1 Pa Ar to remove adsorbed water or other impurities. p_{Ar} was then set to the desired value and the target was cleaned by presputtering using a magnetron gun operated in DC mode at 400 W for 5 min onto a closed shutter. The shutter was then opened to deposit a Ta film to a nominal thickness of 500–600 nm.

Stresses in the as-deposited films were calculated from measurements of substrate curvature and were found to vary from – 1360 to + 1140 MPa as $p_{\rm Ar}$ increased [13]. Phase and texture were characterized using x-ray diffraction [13] with x-rays from a conventional Cu K $_a$ source. Symmetric θ - 2θ scans were conducted over the range $20^{\circ} \le 2\theta \le 80^{\circ}$. Many small peaks close to the nominal locations in the powder diffraction files (Inorganic Crystal Structure Database Collection Codes 53793 and 280872) were found, but by tracking their positions with $p_{\rm Ar}$, and therefore stress, it was possible to assign all of them unambiguously to β -Ta [13]. Rocking curves of the (002) β -Ta peak were performed in the ω geometry by setting the diffractometer to the 2θ angle of the (002) β -Ta peak and rotating the scattering vector from –15 $^{\circ}$ to +15 $^{\circ}$ from the substrate normal in the diffraction plane. The full width at half maximum (FWHM) of the rocking curves increases from 6° to > 30 $^{\circ}$ as the peak height drops across the pressure range. Analysis of these curves [13] showed that nearly all grains are oriented with [001] near the surface normal while the orientation distribution widens with $p_{\rm Ar}$, *i.e.* films have broadening (002) fiber texture. A very minor fraction (\approx 0.1 vol%) of (410) is the only orientation detected that could not be attributed to the (002) texture component.

2.2. Film geometry and structure

For the present study, high-resolution micrographs of the sample surfaces and cross sections were produced using SEM. Samples were cleaved into smaller pieces for analysis and cross section images were obtained by viewing the fractured film surfaces. Sample thicknesses were obtained from the cross-section images. For samples produced with $p_{Ar} = 0.3$, 0.5, and 1.1 Pa, thicknesses

were also determined using Rutherford backscattered spectrometry (RBS) and the RUMP analysis and simulation software [13]. These samples were used to calibrate the SEM thicknesses.

Figure 1 shows SEM micrographs of film surfaces (left) and cross sections (right). Film thicknesses range from 485 to 644 nm (see Table 1). Distinct domed features are visible at the film surface, and the size of these features (in plan view) increases with p_{Ar} . At low p_{Ar} (e.g. 0.5 and 1.1 Pa), these surface features appear long and worm-like, while at higher p_{Ar} (e.g. 2.0 and 2.2 Pa) the features appear only slightly elongated. Film cross-sections show that the grain structure is columnar.

We used a modified intercept method (based on ASTM E112 [15]) to calculate feature size from the plan view SEM images. We counted intercepts (boundaries between features) along 20 randomly oriented lines for each film, with about 20 intercepts per line, using lines of different orientations to average out in-plane feature anisotropy. Figure 2 shows this estimate of feature size $vs.\ p_{Ar}$. As discussed below, the feature size can be assumed to correspond to the grain size. By this measure, grain size increases from 22.5 ± 3.5 nm to 49.2 ± 9.7 nm with increasing sputter pressure. Structural features of the films are summarized in Table 1.

2.3. Resistivity

Sheet resistivity was measured 30 mm from the edge of the substrate using a four-point probe with an inner probe spacing of 1.6 mm and an outer probe spacing of 4.8 mm. Film resistivity was then calculated by multiplying by the measured film thickness. The mean and standard deviation of 7 measurements in each film are shown in Figure 3. The average resistivity value is $169 \pm 5 \,\mu\Omega$ cm and does not vary systematically with ρ_{Ar} .

2.4. Mechanical Properties

A scanning nanoindenter (Hysitron TriboIndenter 900) with a Berkovich tip was used to determine the mechanical properties of the films. Before testing, tip shape and machine compliance calibrations were made using a vitreous silica sample following the Oliver and Pharr method [16]. To find a range where indentations were large enough to avoid surface effects such as roughness, yet small enough to avoid effects due to the substrate, 64 indentations were made with peak loads from 1 to 10 mN distributed so as to produce roughly equal indentation depth spacings. For each indentation, the load was ramped up linearly over 5 s, held constant for 10 s, and then removed in 5 s. The hardness, H, and the indentation modulus, $E_{\rm ind}$, were extracted from the load-depth data from each indentation using the Oliver & Pharr method [16]. After correcting for machine compliance, a power law was fitted to the unloading data from 20 to 95% of the maximum load, $P_{\rm max}$, and the slope of the fit at $P_{\rm max}$ was taken to be the contact stiffness, S. The contact depth, $h_{\rm c}$, which is the distance along the indenter axis that the film material was in contact with the indenter at $P_{\rm max}$ was then given by

$$h_c = h_{\text{max}} - 0.72(P_{\text{max}}/S)$$
 (1)

where h_{max} is the depth at maximum load. We then found the contact area A_c from the calibrated tip shape function $A_c = f(h_c)$, the hardness from

$$H = P_{\text{max}}/A_{\text{c}} \,\,, \tag{2}$$

and the indentation modulus from

$$E_{ind} = \frac{E_S}{(1 - \nu_S^2)} = \left[\frac{2\sqrt{A}}{\sqrt{\pi}S} - \frac{(1 - \nu_t^2)}{E_t} \right]^{-1} , \tag{3}$$

where E and ν are Young's modulus and Poisson's ratio, respectively, and the subscripts s and t refer to the sample and indenter tip respectively, using E_t = 1140 GPa and ν_t = 0.07 for the properties of the diamond tip¹.

Figure 4 shows the calculated hardness and indentation modulus of the film made at 0.3 Pa vs. contact depth. Surface effects are manifest in the reduced hardness below about 25 nm, but hardness is roughly constant above 25 nm. The elastically deformed region is much larger than the plastic region [18], so E_{ind} decreases as h_c increases due to the influence of the substrate (E_{ind} for Si is ≈ 178.6 GPa [19]).

To avoid surface effects and minimize the influence of the substrate, we averaged properties from measurements with contact depths of 40–60 nm from each sample to obtain average hardness and indentation modulus values for each sample. Figures 5a and 5b show the mean and standard deviation of H and $E_{\rm ind}$ values, respectively, calculated from ≈ 10 indentations in each film as a function of p_{Ar} . The hardness decreases continuously with increasing sputter pressure from 16.4 GPa to 11.3 GPa, while the indentation modulus is ~ 209 GPa independent of p_{Ar} for samples deposited at lower pressures, but decreases with increasing p_{Ar} above $p_{Ar} \approx 1.6$ Pa. Scatter in both H and $E_{\rm ind}$ increases with p_{Ar} .

The indenter was also used as an imaging probe in surface force microscopy mode with an imaging force of 2 μ N to obtain the surface topography of the 0.3 and 2.2 Pa samples to investigate possible pileup around the edges of the indentations. Pileup height scaled with indentation load, reaching \sim 8 and \sim 9 nm for indentations made to 160 nm depth in the films deposited at 0.3 and 2.2 Pa, respectively. However, it was small enough to be difficult to measure for the 40–60 nm indentations we used for hardness and modulus calculations. Since the resolution of these measurements is \sim 1 nm and there is no variation with p_{Ar} , we assume pileup has a negligible effect on our calculated hardness and modulus values.

To test for strain rate sensitivity effects, indentations were made to 10 mN at rates that varied from 0.5 to 20 mN/s. This load was held until the indenter stopped moving (displacement rate approached measured drift rate) and the indenter was then unloaded at 2 mN/s. Unloading data

NOTE: Much confusion has been generated by the conflation of $E_{\rm ind}$ with $E_{\rm r}$, the "reduced modulus" defined by Oliver and Pharr [16] as the inverse of the first term in the brackets in Eq. 3. The indentation modulus, $E_{\rm ind}$, as defined in Eq. 3, is an appropriate measure of the elastic response of the tested material obtained in an indentation experiment just as the Young modulus, $E_{\rm s}$ is an appropriate measure of the elastic response in a uniaxial tension test. For an isotropic material, $E_{\rm ind}$ is equivalent to the plane strain modulus, $E_{\rm s}/(1-\nu_s^2)$, also known as the "flexural modulus" (see, e.g. [17]). In contrast, $E_{\rm r}$ is not a material property, but an intermediate value determined by the deformation of both the sample and the indenter tip.

were analyzed using the Oliver and Pharr method as described above. No variations in hardness or modulus with load rate could be detected.

3. DISCUSSION

By varying p_{Ar} while carefully minimizing other sources of variation we obtain a series of virtually 100% β -Ta films with systematic variations in microstructure, allowing us to provide accurate and representative measurements of the properties of the pure β -Ta phase.

3.1. Effect of sputter pressure on microstructure

As is evident in Fig. 1, the grain structure in all of these β -Ta films is columnar. In principle, the elongated surface features at low $p_{\rm Ar}$ could represent either the tops of elongated grains or clusters of small equiaxed (in the film plane) grains. Such elongated surface features in as-deposited β -Ta films have been reported [3]; however, plan view TEM images of β -Ta films invariably show that the grains are equiaxed in the film plane [4–6,20,21], suggesting that each elongated feature is comprised of several individual grains. This is supported by the film deposited at $p_{\rm Ar}$ = 1.6 Pa where roughly equiaxed features, which we take to be grains, are arranged into rows reminiscent of the worm-like surface features in films made at lower $p_{\rm Ar}$. At higher pressures, it is clear that the surface features represent individual grains. For this reason, we treat the feature size as the grain size in Fig. 2. While the fracture surfaces in Fig. 1 are too uneven for statistical analysis, the widths of the measurable columnar features in the high-sputter-pressure films agree with the grain sizes (Fig. 2) obtained from the surface features. We therefore conclude that at all pressures we have columnar, (002)-oriented grains that are approximately equiaxed in the plane of the film. As $p_{\rm Ar}$ increases, the in-plane grain size increases significantly, as the (002) texture distribution widens significantly [13] as well.

The primary means by which p_{Ar} affects thin film structure and properties is through changes in the energies and incident angles of bombarding particles at the substrate caused by collisions with inert gas atoms [13]. These effects are described by "structure zone models," [22] in which the resulting microstructures are mapped out in terms of sputter pressure and homologous substrate temperature, T/T_M , where T_M is the melting point of the film material. These microstructures are divided into four "zones." Zone 1, at low T/T_M and high p_{Ar} , is dominated by atomic shadowing processes, in which surface features prevent material from reaching certain areas of the growing film, and features crystals with high dislocation densities, domed tops, and open, voided, or low-density grain boundaries. Zone 2, at moderate T/T_M and all p_{Ar} , features columnar grains without voids at grain boundaries. Zone 3, at high T/T_M and all p_{Ar} , is dominated by diffusion and features equiaxed grains. Zone T is a transition zone between zones 1 and 2, especially prominent at low sputter pressure, and features highly dislocated crystals with dense boundaries.

According to this model [22], the effects of pressure should be observed primarily in the low-temperature regime, in the transition from Zone 1 to Zone T. As β -Ta is a metastable phase, its melting temperature is not defined, but our deposition temperature of 90°C is low compared to the melting point of α -Ta (3017°C), so we therefore expect our microstructures to be in this regime.

Indeed, the columnar grains and domed tops in Figure 1 are consistent with this model. The model also predicts that at sufficiently high p_{Ar} , sputtered films may start to incorporate voids at grain boundaries [22]. Such voids have been seen in Cr films sputtered under similar conditions [23], but we have no evidence that such voids are present in our films, although we cannot rule them out.

We see an additional effect of sputter pressure that has not been identified in structure zone models: namely, that grain size increases with sputter pressure. This effect has been observed in Cr [23], but no explanation was proposed. We attribute the grain size increase to the decrease in energy of the species incident at the substrate due to increasingly frequent collisions with inert gas atoms as follows:

We have previously calculated the energy per incorporated Ta atom [13], finding values that range from 363 eV/atom at $p_{\rm Ar}$ = 0.3 Pa to 33.8 eV/atom at $p_{\rm Ar}$ = 2.2 Pa. Most of this energy (93% at 0.3 Pa, 50% at 2.2 Pa) was carried by reflected neutrals. We estimated the sputter threshold to be about 81 eV/atom; thus, at least some of the species impinging on the substrate have sufficient energy to resputter Ta atoms from the growing film at $p_{\rm Ar}$ = 0.3 Pa, while much less resputtering can occur at $p_{\rm Ar}$ = 2.2 Pa. We also found that the distribution of incident angles is Gaussian and the width of that distribution increases with $p_{\rm Ar}$

We combined this information with the observation that the β -Ta crystal structure has relatively open channels parallel to [002] to explain the strong (002) texture of the films [13]. To the extent that these channels act as ion channels during deposition, then grains having [002] parallel to the film normal would experience less resputtering than others and would be preferentially preserved. At low p_{Ar} (high energy, low angular distribution), grains with orientations that deviate significantly from (002) are resputtered away, leaving only those with [002] closely aligned with the film normal. At high p_{Ar} (low energy, wider angular distribution), there is little or no resputtering, and a wider set of grain orientations is preserved. Thus, the (002) texture broadens as p_{Ar} increases. As indicated by the (002) rocking curves, the (002) fiber texture component remains constant while the range of angles ψ between {002} and the film normal broadens from about 3° to about 15°.

Without grain size information, we speculated that the final orientation distribution might reflect the orientation distribution of the initial grain nuclei [13]. While this may indeed be the case, knowledge of the grain size may be combined with knowledge of the energy and incident angle distributions, the texture evolution, and the assumption that the mobility is sufficiently low to preclude grain growth by diffusional boundary motion [13], to generate a complete explanation for the increase in grain size with p_{Ar} , as shown in Figure 6, where we consider growth at low p_{Ar} (Fig. 6a–d) and at high p_{Ar} (Fig. 6e–h). At all pressures, we imagine that grain nuclei form with a range of orientations (Fig. 6a and e). In accord with our proposal that β -Ta forms epitaxially on a TaO_x layer [13], the range of initial orientations may be limited. At low p_{Ar} , both the deposition and resputtering rates are high. Initial grains that deviate more than about 3° from perfect (002) orientation are preferentially resputtered away (Fig. 6b). Since the remaining grains have very similar orientations, they grow at the same rate, preserving a fine grain structure (Fig. 6 c and d). At high p_{Ar} , both the deposition and resputtering rates are lower, and the range of incident angles is wide. Thus, there is little or no preferential resputtering, and nuclei with a range of orientations are

preserved (Fig. 6f). However, since different orientations have different growth rates [24], grains with favorable growth orientations (presumably those near (002)) grow at the expense of the others (Fig 6g and h), leading to both larger grains and a wider grain size distribution.

3.2. Resistivity

We observe essentially no change in resistivity over the entire sputter pressure range, despite significant differences in film microstructure. This indicates that the electron mean free path is shorter than the smallest grain size [25]. A simple estimate of the electron mean free path may be calculated from the measured resistivity, atomic mass, and density of the material [26], and for these films is approximately 3.8 Å, on the same order as the interatomic spacing in β -Ta [27] and considerably shorter than the shortest apparent grain diameter.

Other researchers, however, have found that changes in film microstructure do lead to changes in resistivity. Specifically, a few observe that increasing sputter pressure leads to an increase in resistivity [28–30], with a threshold pressure between \sim 1 Pa [28] and \sim 2.6 Pa [30]. This resistivity increase is attributed to the increase in grain boundary voids predicted by the structure zone model, and open spaces between grain boundaries are indeed visible in some of the high-pressure films reported in that work [28]. The insensitivity of our film resistivities to sputter pressure may therefore indicate that void density is negligible in the films reported here, though it is possible for voids to be configured so as to have negligible effect on resistivity [31].

As noted in the Introduction, reported resistivity values for the β phase vary widely (112–1500 μ Ω cm). We attribute this variation to two main sources of error: mixed α and β phases and oxygen impurities. Very low resistivity values can be associated with films having mixed α and β phases since the resistivity of the α phase is much lower (13.1 μ Ω cm). Such films are common and a small amount of α -Ta in a film can dramatically reduce its measured resistivity. For example, Sosniak *et al.* observed up to 15% α -Ta in some samples, but still report resistivities for " β -Ta films" of 112 μ Ω cm [9]. Similarly, Senkevich *et al.* report resistivities of 130-160 μ Ω cm for β -Ta despite the acknowledged presence of small α peaks visible in XRD of films identified as β [10].

Furthermore, it can be quite difficult to determine whether α is present using only symmetric θ -2 θ XRD scans [13]. Typical analyses depend only on diffraction peaks from the main texture components, while less-well-oriented or -diffracting grains may constitute a significant fraction of the film yet produce only very small peaks (orders of magnitude smaller than those from the main texture components. Furthermore, many of the peaks from α - and β -Ta overlap, requiring either a full 3-D texture analysis or some other information to separate them. In our previous study [13], we were able to use shifts in peak positions with stress to make these discriminations. While it is impossible to know what the α -Ta content might have been in films where it wasn't measured or reported, we observe that, in all studies where the resistivity is significantly less than our measured value of $169 \pm 5 \,\mu\Omega$ cm, the presence of α -Ta cannot be ruled out.

Extremely high resistivity values, on the other hand, are associated with oxygen contamination. Tantalum reacts readily with oxygen, and small amounts of incorporated oxygen can have dramatic

effects on film properties [32]. Specifically, oxygen-contaminated Ta has much higher resistivity than either α -Ta or β -Ta [33]. While the oxygen content is not often measured or reported, there are nonetheless several indications that oxygen was present in films having significantly higher resistivities than our measured value of $169 \pm 5 \,\mu\Omega$ cm. For example, Clevenger *et al.* report resistivities of 225-250 μ Ω cm [7], but also observe that their films do not begin to transform to the stable α phase until about 700°C. It has been shown that nominally oxygen-free films transform at about 350°C and that the transformation temperature increases with increasing oxygen content [32]. Clevenger *et al's* transformation behavior [7] looks remarkably like the behavior of β -Ta films with significant oxygen content [32]. Similarly, Solati *et al.* report resistivities of 600-1500 μ Ω cm, but used a base pressure of only 4×10^{-4} Torr [8]. Assuming oxygen is present in a similar ratio as in the atmosphere, this leaves an oxygen partial pressure of about 8×10^{-5} Torr, well within the range shown to affect resistivity [33].

By performing careful phase identification [13] and exercising special care to avoid oxygen, we are able to avoid both of these pitfalls in determining the resistivity of pure β -Ta. Our resistivity value is higher than those of films known to contain α -Ta, and lower than those likely to contain significant oxygen. It is of course possible to obtain resistivity values near ours by having both α -Ta content and oxygen contamination, but by taking pains to minimize both, we believe we have provided the first definitive resistivity value for pure β -Ta.

It is interesting to consider previous studies where deposition procedures (UHV, UHP sputter gas, substrate cleaning, etc. See [13]) might be thought to produce low levels of oxygen contamination. In some (e.g. [34, 35]), resistivity values near ours were reported, suggesting in retrospect that those films were also essentially pure β -Ta, although this was not verified by the x-ray diffraction studies in those reports [13]. In others different values of resistivity were obtained. For example, Ino etal. [816 Ino] worked to produce pure films and, again using an analysis that depended on XRD from only the main texture components, concluded that the resistivity of β -Ta was in the range 120-165 μ Ω cm. Our analysis suggests that their films may have contained varying amounts of α -Ta that were not detected in their XRD analysis.

3.3. Mechanical Properties

The hardness and modulus behavior shown in Fig. 5 can be explained in terms of the variation in microstructure of the β -Ta films with p_{Ar} .

3.3.1. Hardness

As shown in Fig. 5a, the measured hardness of our β -Ta films ranges from 16.4 to 11.3 GPa over the sputter pressure range tested. Figure 7 shows these hardness values plotted vs. the reciprocal square root grain size (from Fig. 2)—i.e. a modified Hall-Petch plot featuring hardness rather than yield strength. A fit of a straight line to these data, in accord with the Hall-Petch relationship,

$$H = H_0 + \frac{k_{HP}}{\sqrt{d}} \,, \tag{4}$$

is also shown, where d is the grain size, $k_{\rm HP}$ = 76 GPa nm^{1/2} the Hall-Petch coefficient, and H_0 = 0.33 GPa the hardness in the absence of grain boundaries.

Fig. 7 also includes data from other studies where films were reported to consist of the β phase and in which both hardness and grain size were reported. Navid *et al.* [3] reported hardnesses from Ta films deposited using sputter gas pressures p_{Ar} from 0.3 to 1.4 Pa. The phase composition of their films varied (a feature attributed to impurities [13]) resulting in a nonmonotonic variation of H with p_{Ar} . Only the films deposited at 0.3 and 0.4 Pa were found to be 100% β -Ta. We recalculated the grain sizes for these two films from their images using the method described in Section 2.1, as their reported grain sizes seem to have been mismeasured [3]. Once corrected, their results agree very well with ours (Fig. 6). Zhang *et al.* [5] also report hardness and grain size values that are close to our Hall-Petch fit.

Others' results do not fall on the same Hall-Petch line. Wang et~al.~[6] and Cao et~al.~[4,20,21] conducted nanoindentation experiments in which hardness values were calculated from load-displacement data obtained at different load rates and reported that load rate significantly affected hardness [4,6]. Cao et~al.~[4] made indentations in which load was ramped up to and back down from a maximum load of 9.8 $\,\mu$ N at fixed rates between 0.098 $\,\mu$ N/s and 9.8 $\,\mu$ N/s without any hold at the maximum load. In previous work [20], they had shown that if the indenter were simply held at the maximum load, a significant amount of time-dependent plastic deformation would occur. It is well known that in such cases, unloading before ongoing plastic deformation is complete can cause significant errors in both hardness and modulus values obtained from an Oliver and Pharr analysis [37], and the variations reported by both groups [4,6] are consistent with such artifacts. In our experiments, with a 10 s hold at maximum load, we did not see any evidence of rate effects on hardness. Wang et~al.~[6] provide no details of their nanoindentation experiments, so it is difficult to evaluate their results.

To include data from Wang *et al.* [6] and Cao *et al.* [4] in Fig 6, we averaged their results from measurements with loading rates between 0.2 and 50 mN/s. Most of these data do not fall on our Hall-Petch curve. Indeed, Cao *et al.* [4] show increasing hardness with grain size. Such reverse Hall-Petch behavior has been reported to occur at small grain sizes in other metals [38] and may be a factor here. Subrahmanyam *et al.* [39] report a hardness of about 20 GPa (no reported error) in a film with very small grains. However, no details of their nanoindentation measurements are given, so these values are difficult to interpret.

Interestingly, Wang et~al.~[6] conducted post-mortem TEM analysis and reported that some of the material in the plastic zone immediately under the indenter had transformed from the beta phase to the alpha phase in the film indented at 5000 $\,\mu$ N/s. Since the phase transformation has been shown to be diffusional in nature [32], such a phase transformation could be responsible for the time dependent behavior reported by Cao et~al.~[4]. This suggests that the β - α phase transformation may play a role in all of the reported hardnesses. Further study of this would be worthwhile.

There do not appear to be any measurements of Hall-Petch constants for β -Ta or similar metals such as β -U or β -W, so we compare with α -Ta and other BCC metals. Cordero *et al.* [40] compiled

grain boundary strengthening data from BCC V, Nb, Ta, Cr, Mo, W and Fe, measured using both hardness testing and tension/compression testing, and using a Tabor factor of 3 to convert between hardness and yield strength measurements. They report tensile test Hall-Petch coefficients between 9.8 (Fe) and 31.6 (W) GPa nm^{1/2} with a coefficient for α -Ta of 24.1 GPa nm^{1/2}. Using the same Tabor factor of 3 to convert our hardness values, our β -Ta Hall-Petch coefficient is essentially identical at 25 GPa nm^{1/2}. This agreement between the $k_{\rm HP}$ values of α - and β -Ta may be fortuitous as there is no reason to expect grain boundary strengthening in the two phases to be the same. Indeed, the reported range of hardnesses for α -Ta (10.2–11.6 GPa [3,39,41]) are significantly lower than the reported range for β -Ta (12.4–20 GPa [3–6,39]).

In principle, there are three other factors that could contribute to the variation in H with p_{Ar} : stresses, anisotropy, and grain boundary voids. However, we do not believe that any of these factors play a major role. Stresses are known to affect hardness and modulus values calculated using the Oliver and Pharr method [16], and the measured stress changes across the pressure range in our films are enormous (Table 1). However, it has also been convincingly demonstrated that such stress-related hardness and modulus variations are artifacts resulting from pileup [42,43]. Since the measured pileup in our films did not change with p_{Ar} , we assume that the changes in hardness with p_{Ar} (Fig. 5a) are not caused by stress.

Cursory inspection of the crystal structure of β -Ta (space group $P\overline{4}2_1m$) suggests that the (001) planes might be the only candidates for low-Peierls-stress slip systems, leading to high plastic anisotropy. Since the orientation distribution broadens with p_{Ar} , one could imagine this anisotropy contributing to the variations in H with p_{Ar} . However, we doubt this explanation because plastic deformation in indentation is well averaged over all directions [44] and, except for special cases where slip systems and indentation faces are well aligned [45], even significant plastic anisotropy leads to small variations in hardness—for example the maximum variation with orientation in Berkovich indentation of HCP Zn is $\sim 20\%$ [44]. Furthermore, it is not evident why variations in H with p_{Ar} due to anisotropy should follow the $1/\sqrt{d}$ dependence seen in Fig. 7.

Voids at grain boundaries, if present, could affect mechanical properties. An increasing void fraction could lower hardness and modulus without significantly affecting resistivity [31] —qualitatively consistent with our results in Fig's 3 and 5. While we can't rule out such effects entirely, we have no direct evidence for the existence of such voids, nor an argument why variations in H with p_{Ar} due to voids should follow a $1/\sqrt{d}$ dependence.

Finally, we note that the scatter in both hardness and indentation modulus values increases systematically with p_{Ar} . Since, even for the largest grain sizes, the indenter is in direct contact with a few dozen grains at maximum load, this seems unlikely to be associated with any inhomogeneity in the sample. Rather, we attribute this to the surface topography. Although the load series results (*e.g.* Fig. 4) suggest that the peak to peak roughness does not change significantly with p_{Ar} , the inplane spacing of the surface features changes with the grain size. As is evident in the film made at $p_{Ar} = 2.2$ Pa in Fig. 1, although the average grain size is much smaller, there are regions where the spacing between the highest points on the tops of the domed grains is 100-200 nm. This corresponds well with the tip radius of ~ 120 nm. Thus, indentations that land on/between groups

of grain peaks will have contact areas that are slightly lower/higher than average, leading to increasing scatter.

3.3.2. Indentation Modulus

The variations in indentation modulus shown in Fig. 5b are much smaller than the variations in hardness (6% vs. 30%) and affect only the samples deposited at higher p_{Ar} . As with hardness, we rule out stress effects because pileup is constant across the sputter pressure range [42,43]. We also continue to neglect the possibility of grain boundary voids at higher p_{Ar} , both because we have no direct evidence of their existence and because the excellent Hall-Petch correlation (Fig. 7) restricts their configurations to those consistent with a $1/\sqrt{d}$ dependence of hardness. Instead, we focus on anisotropy as a possible cause of these variations.

We can assess anisotropy effects by comparing the indentation modulus of our films to the biaxial modulus of nominally identical films measured by substrate curvature as reported by Knepper et al. [46]. Knepper et al's films were deposited in the same system using the same procedure described in Section 2, with a sputter pressure of 1.1 Pa Ar. When measured by substrate curvature, those films had a biaxial modulus $Y = 175 \pm 20$ GPa. For an isotropic material Y = E/(1 - v) and $E_{\text{ind}} = E/(1 - v)$ v^2), so $Y = E_{\text{ind}}(1 - v^2)/(1 - v)$. Using $E_{\text{ind}} = 210.9$ GPa (the value for our 1.1 Pa film) and v = 0.3, we find that if the material were isotropic, we would expect to find Y = 274 GPa based on our nanoindentation results. Since the microstructure and composition of these two films are unlikely to be different, we conclude the difference is the result of anisotropy. Since Y represents in-plane stiffness components while E_{ind} represents some average over all directions [18], and because these films have strong (002) texture, this discrepancy in modulus values suggests that stiffness along the [001] direction is considerably higher than in the (001) plane. This is consistent with the findings of Arakcheeva et al. [27], who report that interatomic distances are approximately 7% shorter in the [001] direction than in any other direction. As interatomic spacing is a strong indicator of stiffness [47], this decreased interatomic spacing could contribute to increased stiffness along the [001] direction. The decrease in E_{ind} with p_{Ar} would reflect this anisotropy because of the pronounced texture broadening that occurs with increased p_{Ar} , (Table 1). As explained above, hardness is not affected by anisotropy to the same degree as modulus.

Modulus is rarely reported for β -Ta. Zhang reports Young's modulus = 193.87 ± 7.40 GPa obtained by nanoindentation [5], but without specifying the Poisson ratio or indenter properties used to calculate this value. If we assume v = 0.3 and calculate Young's modulus from our $E_{\rm ind}$ value from $E_{\rm ind} = E/(1 - v^2)$, we find $E = 189 \pm 2$ GPa, in good agreement with Zhang. Both values are from films with some degree of (002) texture, so high E compared to biaxial modulus in both cases is consistent with our assertion that the [001] direction in β -Ta is stiffer than other directions. Saha et al. [48] report Young's moduli, also obtained using nanoindentation, between about 140 GPa and 250 GPa for β -Ta, but their results seem dominated by substrate effects. In comparison, nanoindentation modulus data of α -Ta films show Young's moduli between 205 and 220 GPa [49], noticeably higher than our calculated Young's modulus value for β -Ta. This is consistent with a study of biaxial moduli in α - and β -Ta, which reported that the biaxial modulus of α -Ta films was more than 50% higher than that of β -Ta films [46]. Similarly, the average interatomic spacing is

significantly longer in β -Ta (average 2.93 Å [27]) than in α -Ta (2.33 Å, calculated from [50]), which should correspond to a decrease in stiffness [51]. Recent work to determine crystal elastic constants of β -Ta using density functional theory calculations as well as experimental measurements using picosecond laser ultrasonics and Brillouin light spectroscopy [52] provide support for both the anisotropy of β -Ta and the reduced stiffness of β -Ta relative to α -Ta.

3.4. The nature of the β -Ta phase

A summary of the properties of β -Ta reveals a number of seemingly non-metallic features: The β phase has high resistivity, a negative temperature coefficient of resistance [53], which is not typically associated with metals [54], a complex crystal structure, is brittle (*e.g.* fracture surfaces in Fig. 1), and has a high Hall-Petch constant. We might therefore think of β -Ta as a metalloid, rather than a metallic phase. This would be similar to the case of grey and white tin, where both are allotropes of pure tin, but white tin is metallic while grey tin is a metalloid [55]. This calls for further investigation into the nature of bonding in β -Ta, and whether there may be covalent character present that may be responsible for its unusual metalloid-like properties.

4. SUMMARY AND CONCLUSIONS

A series of β -Ta films were deposited under sputter pressures from 0.3 to 2.2 Pa. By carefully controlling the deposition environment, we were able to produce a range of virtually 100% β -Ta films with negligible oxygen content and wide variations in microstructure and properties.

Grain size increases from 22.5 ± 3.5 nm to 49.2 ± 9.7 nm with increasing sputter pressure, which can be explained based on the energy and incident angle distributions of species incident on the growing film during deposition. At low p_{Ar} , grains with orientations different from (002) are resputtered away, leaving only small (002)-oriented grains to grow uniformly. At high p_{Ar} , resputtering is not important, and grains with a range of orientations grow competitively resulting in larger grains with a broader orientation distribution.

Nanoindentation hardness varies from 16.4 to 11.3 GPa with sputter pressure and is correlated with grain size consistent with Hall-Petch behavior. Data from others follow the same relationship except for very small grain sizes, explaining the wide range of reported values. The Hall-Petch constant agrees well with those of BCC metals. In broad terms, the structures, stresses, grain sizes, and hardnesses of β -Ta are similar across many studies, and show that beta is significantly harder than alpha. The beta phase is also significantly more compliant. The indentation modulus of highly textured (002) β -Ta is about 209 GPa and the stiffness is anisotropic, being considerably higher in the [001] direction than in directions perpendicular to [001].

We have obtained a reference value for the resistivity of relatively oxygen-free pure β -Ta of 169 ± 5 μ Ω cm. Lower reported values are attributed to presence of the low-resistivity α phase and higher values to the presence of oxygen. Variations in hardness and modulus arise from variations in grain size and orientation, which are in turn due to variations in the sputter pressure and not due to variations in phase composition, oxygen content, impurities, which have been reported in

previous studies. While we can't completely rule out the effect of grain boundary voids on hardness and modulus, their effects, if any, appear to be minor.

These values for grain size, hardness, modulus, and resistivity thus accurately describe the behavior of relatively oxygen-free pure β -Ta for the first time.

5. ACKNOWLEDGMENTS

Support for this work was provided by the National Science Foundation (DMR 1106223 and DMR 1810138). This work also made use of the facilities of the Cornell Center for Materials Research with support from the National Science Foundation Materials Research Science and Engineering Centers program (DMR 1120296 and DMR 1719875). We also thank Hysitron, Inc. (now Bruker Nano Surfaces) for support of the nanoindentation experiments.

6. REFERENCES

- [1] M.H. Read, C. Altman, A new structure in tantalum thin films, Appl. Phys. Lett. 7 (1965) 51–52. doi:https://doi.org/10.1063/1.1754294.
- [2] W.D. Westwood, F.C. Livermore, Phase composition and conductivity of sputtered tantalum, Thin Solid Films. 5 (1970) 407–420. doi:10.1016/0040-6090(70)90112-4.
- [3] A.A. Navid, A.M. Hodge, Nanostructured alpha and beta tantalum formation—Relationship between plasma parameters and microstructure, Mater. Sci. Eng. A. 536 (2012) 49–56. doi:10.1016/j.msea.2011.12.017.
- [4] Z. Cao, Q. She, Y. Huang, X. Meng, The rate sensitivity and plastic deformation of nanocrystalline tantalum films at nanoscale, Nanoscale Res. Lett. 6 (2011) 2–7. doi:10.1186/1556-276X-6-186.
- [5] M. Zhang, Y.F. Zhang, P.D. Rack, M.K. Miller, T.G. Nieh, Nanocrystalline tetragonal tantalum thin films, Scr. Mater. 57 (2007) 1032–1035. doi:10.1016/j.scriptamat.2007.07.041.
- [6] Y.M. Wang, A.M. Hodge, P.M. Bythrow, T.W. Barbee, A. V. Hamza, Negative strain rate sensitivity in ultrahigh-strength nanocrystalline tanta um, Appl. Phys. Lett. 89 (2006) 2004–2007. doi:10.1063/1.2338006.
- [7] L.A. Clevenger, A. Mutscheller, J.M.E. Harper, C. Cabral, K. Barmak, The relationship between deposition conditions, the beta to alpha phase transformation, and stress relaxation in tantalum thin films, J. Appl. Phys. 72 (1992) 4918–4924. doi:10.1063/1.352059.
- [8] E. Solati, D. Dorranian, Investigation of the Structure and Properties of Nanoscale Grain-Size β -Tantalum Thin Films, Mol. Cryst. Liq. Cryst. 571 (2013) 67–76. doi:10.1080/15421406.2012.741347.
- [9] J. Sosniak, W.J. Polito, G.A. Rozgonyi, Effect of Background-Gas Impurities on the Formation of Sputtered β-Tantalum Films, J. Appl. Phys. 38 (1967) 3041. doi:10.1063/1.1710059.
- [10] J.J. Senkevich, T. Karabacak, D.-L. Bae, T.S. Cale, Formation of body-centered-cubic tantalum via sputtering on low-k dielectrics at low temperatures, J. Vac. Sci. Technol. B Microelectron. Nanom. Struct. 24 (2006) 534–538. doi:10.1116/1.2166860.
- [11] L. Liu, C.-F.F. Pai, Y. Li, H.W. Tseng, D.C. Ralph, R.A. Buhrman, Spin-Torque Switching with the Giant Spin Hall Effect of Tantalum, Science. 336 (2012) 555–558. doi:10.1126/science.1218197.
- [12] W.D. Westwood, N. Waterhouse, Structure and Electrical Properties of Tantalum Films Sputtered in Oxygen-Argon Mixtures, J. Appl. Phys. 42 (1971) 2946–2952. doi:https://doi.org/10.1016/0040-6090(72)90273-8.
- [13] E.A.I. Ellis, M. Chmielus, S.P. Baker, Effect of sputter pressure on Ta thin films: Beta phase selection, texture, and stress, Acta Mater. 150 (2018) 317–326. doi:https://doi.org/10.1016/j.actamat.2018.02.050.
- [14] J.B. Shu, S.S. Clyburn, T.E. Mates, S.P. Baker, Effect of oxygen on the thermomechanical behavior of passivated Cu thin films, J. Mater. Res. 18 (2003) 2122–2134. doi:https://doi.org/10.1557/JMR.2003.0298.
- [15] ASTM E112-13, Standard Test Methods for Determining Average Grain Size, ASTM International, West Conshohocken, PA, 2013.

- [16] W.C.C. Oliver, G.M.M. Pharr, An improved technique for determining hardness and elastic modulus using load and displacement sensing indentation experiments, J. Mater. Res. 7 (1992) 1564–1583. doi:10.1557/JMR.1992.1564.
- [17] S.P. Baker, W.D. Nix, Mechanical Properties of compositionally-modulated Au-Ni thin films: nanoindentation and micro-cantilever beam deflection experiments, J. Mater. Res. 9 (1994) 3131–3144. doi:https://doi.org/10.1557/JMR.1994.3131.
- [18] R.P. Vinci, J.J. Vlassak, Mechanical Behavior of Thin Films, Annu. Rev. Mater. Sci. 26 (1996) 431–462. doi:https://doi.org/10.1146/annurev.ms.26.080196.002243.
- [19] H. Li, J.J. Vlassak, Determining the elastic modulus and hardness of an ultra-thin film on a substrate using nanoindentation, J. Mater. Res. 24 (2009) 1114–1126. doi:10.1557/jmr.2009.0144.
- [20] Z.H. Cao, P.Y. Li, H.M. Lu, Y.L. Huang, Y.C. Zhou, X.K. Meng, Indentation size effects on the creep behavior of nanocrystalline tetragonal Ta films, Scr. Mater. 60 (2009) 415–418. doi:10.1016/j.scriptamat.2008.11.016.
- [21] Z.H. Cao, P.Y. Li, X.K. Meng, Nanoindentation creep behaviors of amorphous, tetragonal, and bcc Ta films, Mater. Sci. Eng. A. 516 (2009) 253–258. doi:10.1016/j.msea.2009.03.019.
- [22] J.A. Thornton, High rate thick film growth, Annu. Rev. Mater. Sci. 7 (1977) 239–260. doi:10.1146/annurev.ms.07.080177.001323.
- [23] S.Y. Grachev, F.D. Tichelaar, G.C.A.M. Janssen, Stress in sputter-deposited Cr films: Influence of Ar pressure, J. Appl. Phys. 97 (2005) 073508. doi:10.1063/1.1876579.
- [24] I. Petrov, P.B. Barna, L. Hultman, J.E. Greene, Microstructural evolution during film growth, J. Vac. Sci. Technol. A Vacuum, Surfaces, Film. 21 (2003) S117–S128. doi:10.1116/1.1601610.
- [25] S. Kasap, P. Capper, Electrical Conduction in Metals and Semiconductors, in: Springer Handb. Electron. Photonic Mater., Springer, Boston, MA, 2007: pp. 19–45.
- [26] U. Mizutani, Introduction to the Electron Theory of Metals, Cambridge University Press, 2001.
- [27] A. Arakcheeva, C. Gervais, V. Grinevitch, The self-hosting structure of beta-Ta, Acta Crystallogr. Sect. B. B58 (2002) 1–7. doi:https://doi.org/10.1107/S0108768101017918.
- [28] M. Grosser, U. Schmid, The impact of sputter conditions on the microstructure and on the resistivity of tantalum thin films, Thin Solid Films. 517 (2009) 4493–4496. doi:10.1016/j.tsf.2008.12.009.
- [29] W.D. Westwood, R.J. Boynton, P.S. Wilcox, The Effects of Argon Pressure on the Properties of Sputtered Tantalum Films, Thin Solid Films. 16 (1973) 1–25. doi:https://doi.org/10.1016/0040-6090(73)90154-5.
- [30] J.A. Thornton, D.W. Hoffman, Internal stresses in titanium, nickel, molybdenum, and tantalum films deposited by cylindrical magnetron sputtering, J. Vac. Sci. Technol. 14 (1977) 164. doi:10.1116/1.569113.
- [31] T. Sun, B. Yao, A.P. Warren, K. Barmak, M.F. Toney, R.E. Peale, K.R. Coffey, Surface and grain-boundary scattering in nanometric Cu films, Phys. Rev. B Condens. Matter Mater. Phys. 81 (2010) 1–12. doi:10.1103/PhysRevB.81.155454.

- [32] R. Knepper, B. Stevens, S.P. Baker, Effect of oxygen on the thermomechanical behavior of tantalum thin films during the β - α phase transformation, J. Appl. Phys. 100 (2006) 123508. doi:10.1063/1.2388742.
- [33] A. Schauer, M. Roschy, R.F. sputtered β -tantalum and b.c.c. tantalum films, Thin Solid Films. 12 (1972) 313–317. doi:10.1016/0040-6090(72)90095-8.
- [34] P. Catania, J.P. Doyle, and J.J. Cuomo, Low Resistivity Body-Centered Cubic Tantalum Thin-Films as Diffusion-Barriers between Copper and Silicon. J. Vac. Sci. Technol. A, 10 (1992) 3318-3321.
- [35] J.J. Colin, G. Abadias, A. Michel, and C. Jaouen, On the origin of the metastable beta-Ta phase stabilization in tantalum sputtered thin films. Acta Mater. 126 (2017) 481-493. doi: 10.1016/j.actamat.2016.12.030
- [36] K.T. Ino, T. Shinohara, T. Ushiki, and T. Ohmi, Ion energy, ion flux, and ion species effects on crystallographic and electrical properties of sputter-deposited Ta thin films. J. Vac. Sci. Technol. A, 15 (1997) 2627.
- [37] S.P. Baker, T.W. Barbee, W.D. Nix, Time-dependent deformation in room-temperature indentation experiments using a nanoindenter, in: Thin Film. Stress. Mech. Prop. III, Materials Research Society, Boston, MA, U.S.A., 1992: pp. 319–324. doi:https://doi.org/10.1557/PROC-239-319.
- [38] C.E. Carlton, P.J. Ferreira, What is behind the inverse Hall-Petch effect in nanocrystalline materials?, Acta Mater. 55 (2007) 3749–3756. doi:10.1016/j.actamat.2007.02.021.
- [39] A. Subrahmanyam, K. Valleti, S. V Joshi, G. Sundararajan, Effect of arc suppression on the physical properties of low temperature dc magnetron sputtered tantalum thin films, J. Vac. Sci. Technol. A Vacuum, Surfaces, Film. 25 (2007) 378. doi:10.1116/1.2699296.
- [40] Z.C. Cordero, B.E. Knight, C.A. Schuh, Six decades of the Hall-Petch effect a survey of grain-size strengthening studies on pure metals, Int. Mater. Rev. 61 (2016) 495–512. doi:https://www.tandfonline.com/author/Schuh%2C+C+A.
- [41] M. Zhang, B. Yang, J. Chu, T. Nieh, Hardness enhancement in nanocrystalline tantalum thin films, Scr. Mater. 54 (2006) 1227–1230. doi:10.1016/j.scriptamat.2005.12.027.
- [42] T.Y. Tsui, W.C. Oliver, G.M. Pharr, Influences of stress on the measurement of mechanical properties using nanoindentation: Part I. Experimental studies in an aluminum alloy, J. Mater. Res. 11 (1996) 752–759. doi:10.1557/JMR.1996.0091.
- [43] A. Bolshakov, W.C. Oliver, G.M. Pharr, Influences of stress on the measurement of mechanical properties using nanoindentation: Part II. Finite element simulations, J. Mater. Res. 11 (1996) 760–768. doi:https://doi.org/10.1557/JMR.1996.0092.
- [44] J.J. Vlassak, W.D. Nix, Measuring the Elastic Properties of Anisotropic Materials by Means of Indentation, J. Mech. Phys. Solids. 42 (1994) 1223–1245. doi:https://doi.org/10.1016/0022-5096%2894%2990033-7.
- [45] J. Carloni, Mechanical Deformation and Strengthening Mechanisms in Calcite Single Crystals, Doctoral dissertation, Cornell University, Cornell University, 2017.
- [46] R. Knepper, S.P. Baker, Coefficient of thermal expansion and biaxial elastic modulus of β phase tantalum thin films, Appl. Phys. Lett. 90 (2007) 181908. doi:10.1063/1.2734468.

- [47] W.D.J. Callister, D.G. Rethwisch, Materials Science and Engineering, 9th ed., John Wiley & Sons, Inc., Hoboken, N.J., 2014.
- [48] R. Saha, J.A. Barnard, Effect of structure on the mechanical properties of Ta and Ta(N) thin films prepared by reactive DC magnetron sputtering, J. Cryst. Growth. 174 (1997) 495–500. doi:10.1016/S0022-0248(96)01148-7.
- [49] F. Ferreira, C. Sousa, A. Cavaleiro, A. Anders, J. Oliveira, Phase tailoring of tantalum thin films deposited in deep oscillation magnetron sputtering mode, Surf. Coatings Technol. 314 (2017) 97–104. doi:10.1016/j.surfcoat.2016.08.017.
- [50] M.H. Mueller, The lattice parameter of tantalum, Scr. Metall. 11 (1977) 693. doi:10.1016/0036-9748(77)90141-7.
- [51] K. Fuchs, H.W. Peng, Crystal theory of metals: calculation of the elastic constants, Proc. R. Soc. London. Ser. A. Math. Phys. Sci. 180 (1942) 451–476. doi:10.1098/rspa.1942.0050.
- [52] G. Abadias, J.J. Colin, D. Tingaud, P. Djemia, L. Belliard, and C. Tromas, Elastic properties of α -and β -tantalum thin films. Thin Solid Films, 688 (2019) 137403. doi: 10.1016/j.tsf.2019.06.053
- [53] N. Schwartz, W.A. Reed, P. Polash, M.H. Read, Temperature coefficient of resistance of beta-tantalum films and mixtures with b.c.c.-tantalum, Thin Solid Films. 14 (1972) 333–347. doi:10.1038/467S2a.
- [54] N.N. Kovaleva, D. Chvostova, A. V. Bagdinov, M.G. Petrova, E.I. Demikhov, F.A. Pudonin, A. Dejneka, Interplay of electron correlations and localization in disordered b -tantalum films: Evidence from dc transport and spectroscopic ellipsometry study, Appl. Phys. Lett. 051907 (2015) 1–5. doi:10.1063/1.4907862.
- [55] L. Pauling, Metallic Valence, in: Gen. Chem. 3rd Ed., 1970: p. 586.

7. TABLES

Table 1: Summary of film deposition parameters and properties.

Table 1

$p_{ m Ar}$		Thickness	FWHM rocking	Stress	Grain size	Hardness	$E_{ m ind}$	ρ
[Pa]	[mTorr]	[nm]	[°]	[MPa]	[nm]	[GPa]	[GPa]	[μΩcm]
0.3	2	485	5.43	-1358	22.5±3.5	16.4±0.1	209.3±2.1	172±11
0.5	4	505	5.73	-1045	23.0±3.7	16.2±0.1	209.9±1.3	163±9
1.1	8	601	7.61	-641	26.1±3.3	15.6±0.2	210.9±2.8	169±7
1.6	12	611	11.27	-216	27.3±4.5	14.6±0.2	210.3±2.1	172±7
1.9	14	616	16.09	179	30.4±3.4	13.4±0.2	206.7±2.8	163±6
2.0	15	644	24.66	544	37.1±6.8	12.9±0.4	207.7±2.2	167±7
2.2	16	638	30.26	1149	49.2±9.7	11.3±0.5	197.6±5.1	177±7

8. FIGURE CAPTIONS

- Figure 1: SEM micrographs of β -Ta films deposited at different sputter pressures. Left: plan view surface images. Right: cross sections of films made by viewing cleaved samples.
- Figure 2: Grain size (as determined by line intercept method) of β -Ta films *vs.* Ar sputter pressure. Grain size increases systematically with sputter pressure.
- Figure 3: Resistivity of β -Ta films vs. sputter pressure. Resistivity is not sensitive to p_{Ar} over this range.
- Figure 4: Hardness and indentation modulus *vs.* contact depth for the film deposited at 0.3 Pa. Indentations with $40 \le h_c \le 60$ nm were assumed to be large enough to avoid surface effects while minimizing the influence of the substrate.
- Figure 5: (a) Hardness and (b) indentation modulus vs. sputter pressure. H decreases with increasing p_{Ar} , while E_{ind} is insensitive to p_{Ar} at low pressures, but drops slightly for the films deposited with $p_{Ar} > 1.6$ Pa.
- Figure 6: Proposed grain evolution model for films deposited at low and high sputter gas pressure, p_{Ar} . At low pressure, initial grain embryos (a) are subjected to high-energy bombarding species that selectively resputter poorly-oriented grains (b), which are then replaced by new (002) grains (c), leading to a fine, columnar grain structure with sharp (002) fiber texture (d). At high pressure, poorly-oriented grains (e) are not resputtered (f), but grow more slowly and are overgrown by their better-oriented neighbors (g), leading to a coarser-grained structure with less-sharply oriented (002) texture (h).
- Figure 7: Hall-Petch analysis of hardness data from Fig. 4: hardness increases linearly with reciprocal of the square root of grain size with slope 76 GPa nm^{1/2} (Hall-Petch coefficient), intercept 0.33 GPa (single crystal strength), and coefficient of determination $R^2 = 0.97$. Also shown: data for β -Ta films from Navid *et al.* [3], Cao *et al.* [4], Zhang *et al.* [5], Subrahmanyam *et al.* [36], and Wang *et al.* [6].

9. FIGURES

Figure 1

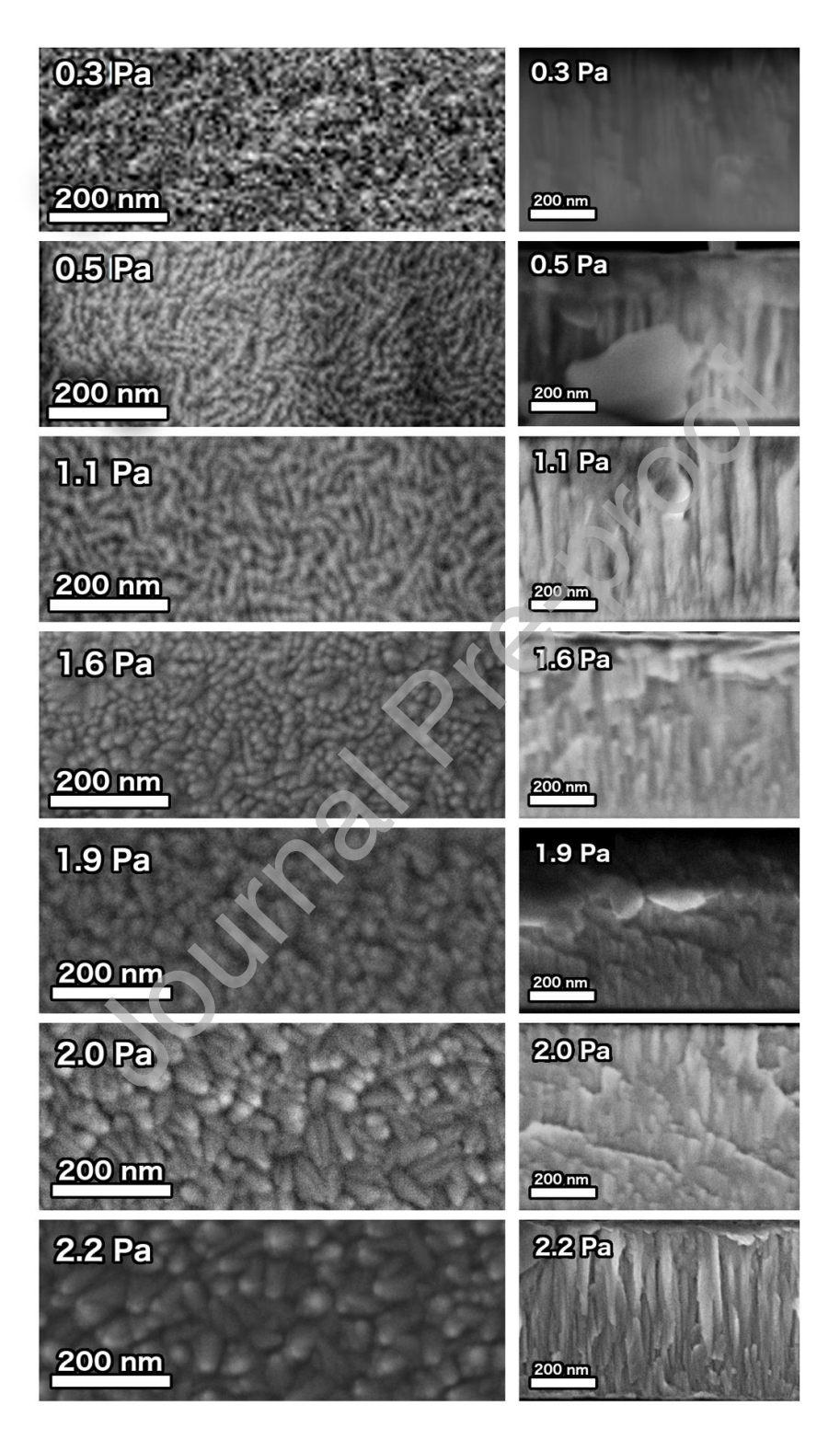


Figure 2

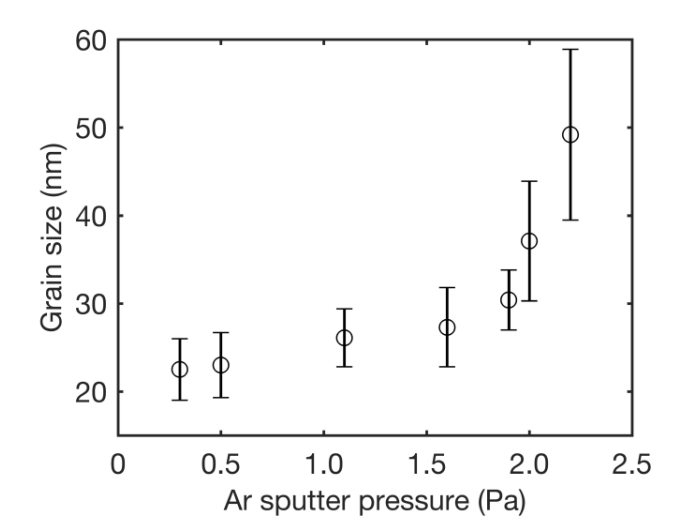


Figure 3

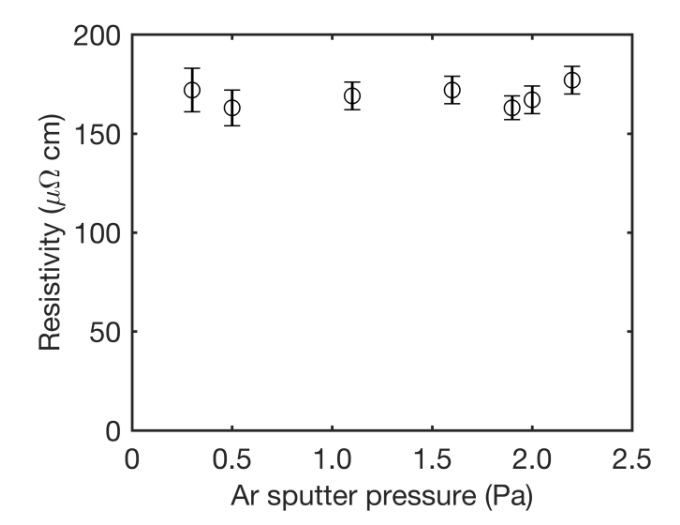


Figure 4

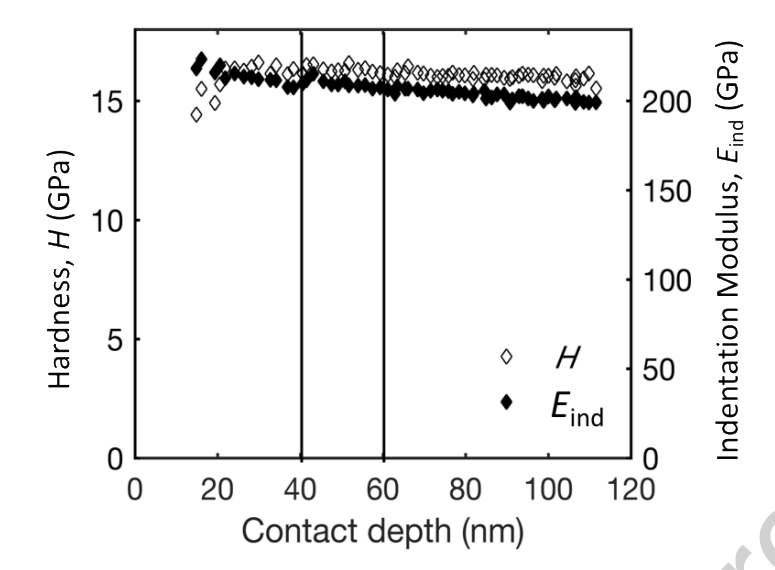
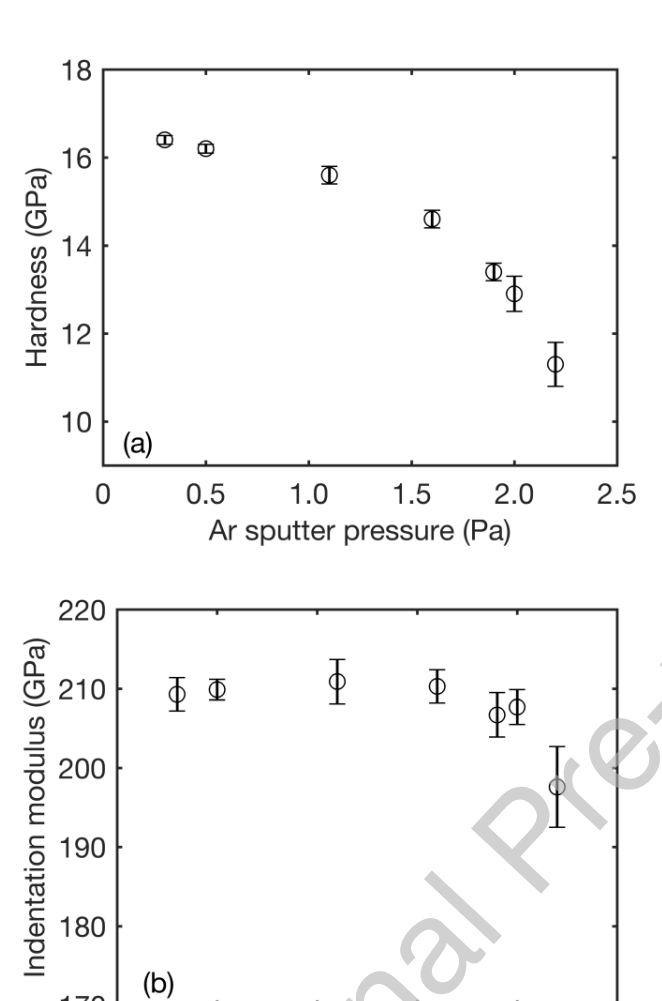


Figure 5

170

0

0.5



0.5 1.0 1.5 2. Ar sputter pressure (Pa)

2.0

2.5

Figure 6

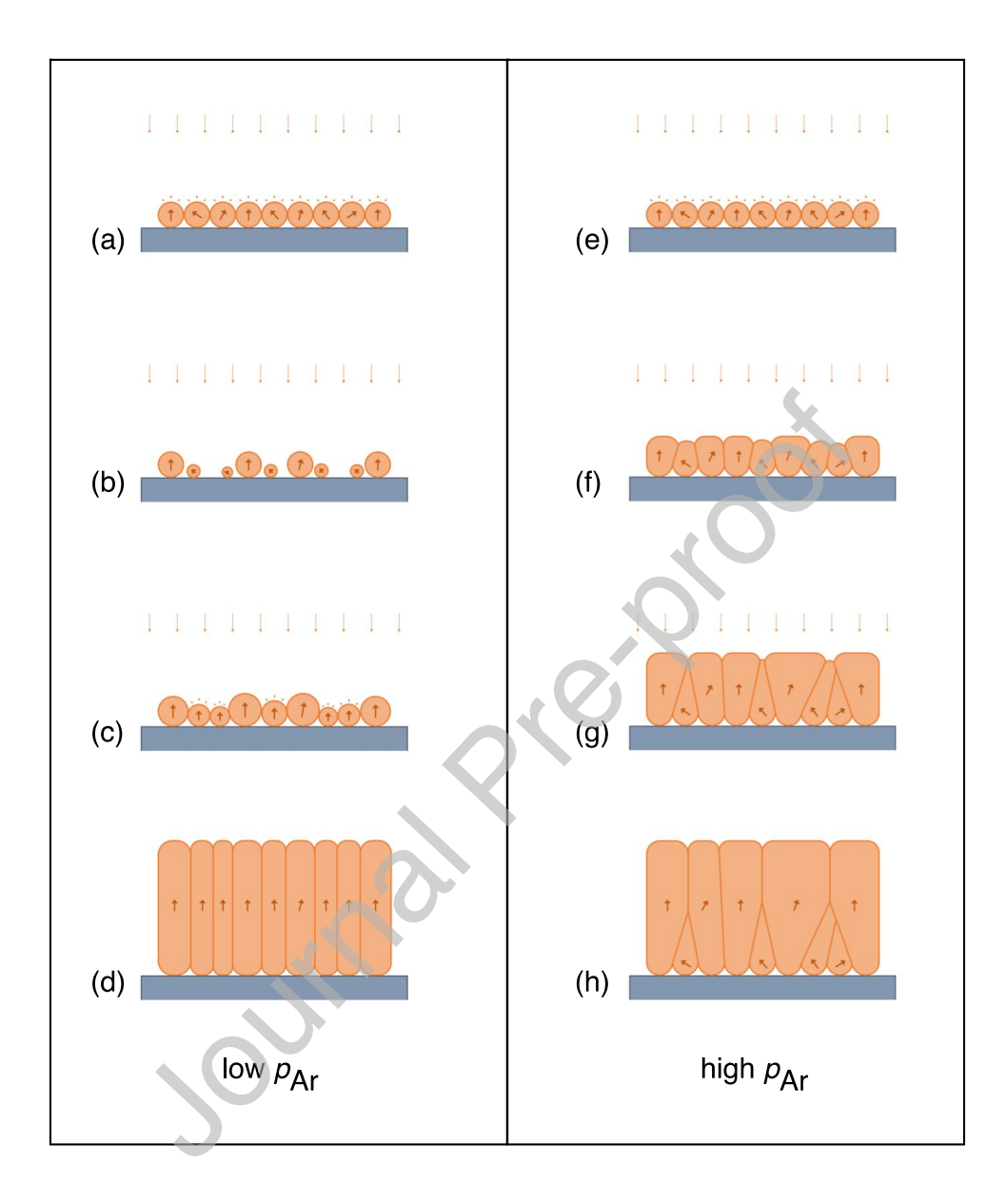
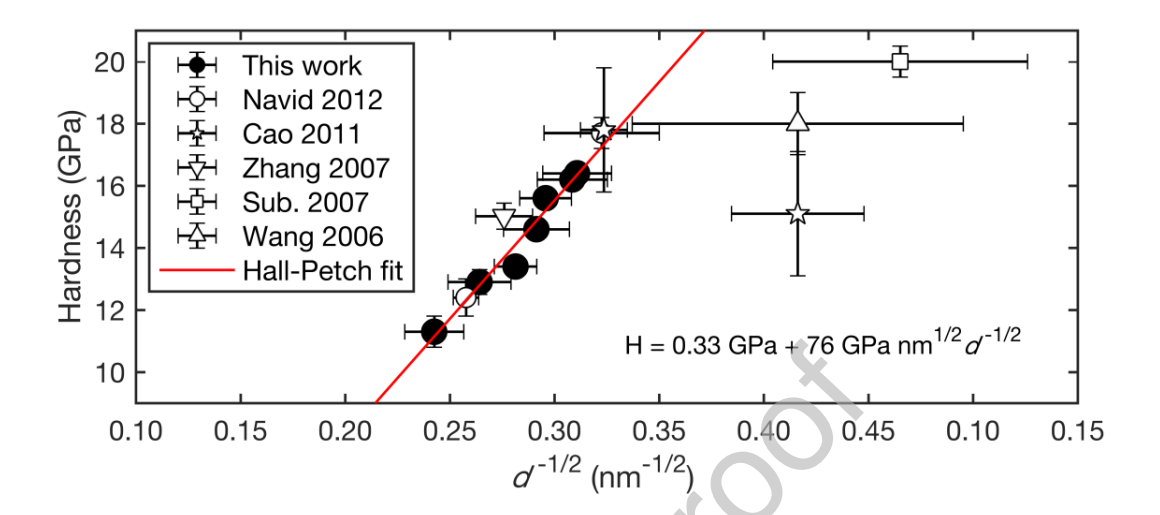


Figure 7.



Graphical abstract

